Scripta Materialia 140 (2017) 67–70

Contents lists available at ScienceDirect

Scripta Materialia

journal homepage: www.elsevier.com/locate/scriptamat

Regular article

Orientation imaging of macro-sized polysilicon grains on wafers using spatially resolved acoustic spectroscopy☆

Rikesh Patel*, Wenqi Li, Richard J. Smith, Steve D. Sharples, Matt Clark

Optics and Photonics Group, Faculty of Engineering, University of Nottingham, University Park, Nottingham NG7 2RD, UK

ARTICLE INFO

Article history:
Received 12 June 2017
Received in revised form 4 July 2017
Accepted 6 July 2017
Available online 14 July 2017

Keywords:
Acoustic methods
Solar cells
Crystal structure
Microstructure
Nondestructive testing

ABSTRACT

Due to its economical production process polysilicon, or multicrystalline silicon, is widely used to produce solar cell wafers. However, the conversion efficiencies are often lower than equivalent monocrystalline or thin film cells, with the structure and orientation of the silicon grains strongly linked to the efficiency. We present a non-destructive laser ultrasonic inspection technique, capable of characterising large (52 × 76 mm^2) photocell's microstructure - measurement times, sample surface preparation and system upgrades for silicon scanning are discussed. This system, known as spatially resolved acoustic spectroscopy (SRAS) could be used to optimise the polysilicon wafer production process and potentially improve efficiency.

1. Introduction

Most manufactured crystalline silicon solar cells available can be categorised as either mono-crystalline (i.e. single crystal) or multi-crystalline (mc-Si), also known as polysilicon. Whilst single crystal solar cells are usually more efficient, most processes commonly used in creating them (e.g. the Czochralski process) can be expensive, time consuming and energy intensive. It has been reported that polysilicon wafers account for around 65% of the solar cell market due to their economical production costs [1]. An important challenge for developers is in increasing polysilicon solar cell efficiency - currently, figures of > 21% have been achieved [2,3]. A well known method of improving the conversion efficiency involves controlling the microstructure of the polysilicon ingots during the directional solidification (DS) process [4–6]. High dislocation densities result in increased recombination rates (affecting the cell lifetime and efficiency), with nearby grain sizes a key factor determining the density [7,8]. Some studies also report on the dislocation densities in relation to the predominant orientation of nearby grains [6,9,10]. In order to optimise the quality of manufactured silicon cells, measuring the grain structure of the material becomes an integral part of the process control. Requirements of such a polysilicon measurement technique could include for it to be non-destructive, economical, safe for workshop environments, and free from measurement size restrictions.

Many methods exist to determine material grain sizes, including nanoscale measurements using scanning electron microscopy (SEM) [11] or X-ray based methods [12], and rapid optical imaging techniques [13,14]. However, only a limited number of inspection techniques exist capable of accurately determining material grain orientation. The most well known is characterisation using electron back scatter diffraction (EBSD) [15,16] - the major advantage of using EBSD is its resolution, both spatial (<10 nm) and angular (<1°) [17]. However, there is a heavy expense associated with the system, operation and maintenance. Additionally, the measured samples are subject to extreme restrictions on size and surface finishing. Another well used method of grain characterisation is X-ray diffraction (XRD), such as one based on Laue back scattered diffraction [18]. In work presented by Lehmann et al., a system was developed that determined grain boundaries optically, with a Laue scanner measuring a single point in each grain to determine the overall sample microstructure. The scan time was 5 h on a 156 × 156 mm^2 silicon wafer, with the sample size limited by the motorised translation stage.

In this paper, we present a laser ultrasonic inspection method capable of determining the grain orientation of silicon wafers. The presented method is known as spatially resolved acoustic spectroscopy, or SRAS [19], and has in the past been used to characterised the microstructure of metals and alloys [20,21]. SRAS is capable of

☆ All authors have equally contributed to this document.

* Corresponding author.
E-mail address: rikesh.patel@nottingham.ac.uk (R. Patel).

http://dx.doi.org/10.1016/j.scriptamat.2017.07.003

rapid scanning, and is an all-optical measurement system - we have adapted this technique to produce microstructure images on silicon.

2. Spatially resolved acoustic spectroscopy

SRAS is a non-contact, non-destructive evaluation (NDE) technique which probes the surface of materials using surface acoustic waves (SAW). The technique has been described in detail previously [19–21] but to-date it has not been used to image silicon - a brief system description is given in this section.

A surface acoustic wave is generated using a pulsed laser, patterned by an optical mask, and imaged onto the sample surface. The patterned absorption of laser energy through the thermo-elastic effect creates a surface wave, the frequency of which, f_s, is determined by the period (i.e. separation) of the grating fringes, or grating wavelength, λ_g, and the SAW velocity, v_s, which is dictated by the material properties, such that;

$$v_s = f_s \lambda_g \tag{1}$$

A second laser is used to measure the surface perturbation due to the propagating SAW - the frequency, f_s, is measured and the SAW velocity, v_s, is calculated. The frequency within the wave packet does not change once the wave begins to propagate - the frequency measured is determined by the surface properties *where the SAW is generated*, and can be detected anywhere along the propagation path, making this a very robust measurement as it does not rely on time of flight and is immune to acoustic aberrations [19]. Fig. 1 illustrates a simple schematic of the SRAS system.

In the current SRAS system, the generation laser is an AOT IR (1064 nm) Q-switched laser (AOT-YAG-10Q) with pulse widths of 1–2 ns and energies of 50–150 μJ, with a repetition rate of 2 kHz. The detection laser is a Laser Quantum (532 nm) continuous wave laser (Torus 532) with an output of 200 mW, which is fibre coupled into the optical setup. The sample is scanned using x-y stages (Physik Instrumente motorised translation stages), and their travel dictates the output images' pixel size - the measurement scan area can be up to 300 × 300 mm^2. For the work presented in this paper, the detection spot was focused down to $\tilde{\varnothing}8\ \mu m$ and the generation patch was $\tilde{\varnothing}200\ \mu m$ on the sample. The grating wavelength, λ_g, used was 24 μm. An optical intensity return is also obtained from each scan point, producing a similar output to that of a scanning optical microscope. The scan speed is limited by the generation laser repetition rate, ADC unit acquisition speed, and translation stage speed - with measurement overheads, the scan speed is typically 1000–1500 points⁄s depending on the detector used.

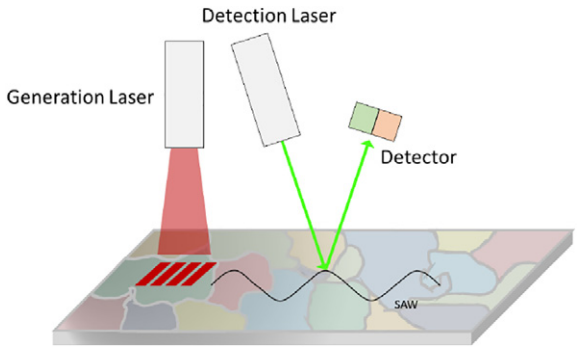

Fig. 1. A schematic of the SRAS operation - a surface acoustic wave is generated and detected using separate lasers, with the perturbation due to the wave picked up using a detector.

3. Finding the orientation

A material's crystallographic grain orientation, the material's elastic constants, and the velocity of a propagating acoustic wave on the material are all intimately related; knowledge of any two of these allows the determination of the third. Generally, the elastic constants for a material are obtained from the literature, or by complementary techniques, and the velocity is measured experimentally (here by the SRAS technique) - this information is sufficient to determine the grain orientation. The process of directly determining the orientation (the inverse problem) is difficult to solve, so fitting is used [20].

Briefly, the expected velocity for each possible orientation is calculated using the material's known elastic constants and density. This data is available in literature - for silicon, these are $C_{11} = 165$ GPa, $C_{12} = 64$ GPa, $C_{44} = 79.2$ GPa, and $\rho = 2.328$ g cm^{-3} [22]. The calculation takes into account the possible wave modes that could be present and applies weightings related to the instrument's ability to detect them (i.e. by the amount of out of plane motion) - this creates a database of dominant velocities for each orientation. The measured SAW velocity is then compared with this database of velocities using a cross correlation algorithm to find the orientation of best fit. This is repeated for each spatial position and the resultant orientation map (presented as an inverse pole figure) is output. The accuracy of the fitting process depends upon the number of directions in which the velocity is measured, the anisotropic ratio for the material, and the SNR of the velocity measurements.

4. Methodology and results

The SRAS instrument in its current form was designed for use on predominantly aerospace materials. The optical wavelengths of the generation and detection lasers are not suitable for direct measurements on silicon. Additionally, the detection system requires an optically smooth surface finish (this is a limitation of the available machine only, and not the SRAS technique in general).

The silicon cells used in this study were commercially available polysilicon panels and required some preparation. The panels were disassembled, the rear screen print coating was removed, and the samples manually polished down to reveal the silicon layer and to give a smooth surface for inspection. For compatibility with the lasers, a thin layer of chromium (~150 nm) was sputter coated on top of the polished silicon. The layer thickness is only a small fraction of the sensing depth of the measurement, which is approximately one acoustic wavelength ($\lambda_a = 24$ μm), and therefore will have a negligible impact on the velocity measurement.

SRAS orientation maps of two sets of silicon cells are presented in this paper. The first (i) is of a fragmented silicon cell, mounted to fit on a $\tilde{\varnothing}2.54$ mm EBSD sample holder. The second (ii) is of two larger 52mm × 38 mm cells. The intention behind presenting the scan data from these samples is to a) compare results obtained using SRAS against an established orientation characterisation technique and to b) display SRAS's ability to scan a large area of material effectively.

The acoustic wavelength used was 24 μm and the samples were scanned with steps of 50 μm and 20 μm along the x-axis and y-axis respectively, creating a 480 × 1200 scan of sample (i), and a 1100 × 4000 scan of sample (ii). To create the orientation maps, shown in Fig. 2 (a) for sample (i) and Fig. 3 for sample (ii), data was taken at each point with the SAW propagating in 9 directions - the time taken to scan each direction was 14 min for sample (i) and 32 min for sample (ii). Both orientation maps show identifiable and contrasting grain shapes and orientations.

To evaluate the measurements collected by SRAS on silicon, a section of sample (i) (highlighted in Fig. 2 (a)) had been analysed using an EBSD instrument (JEOL 7100F FEG-SEM). For comparison, the image generated using data collected by SRAS in this section of sample (i) is shown in Fig. 2 (b) with the EBSD image obtained shown

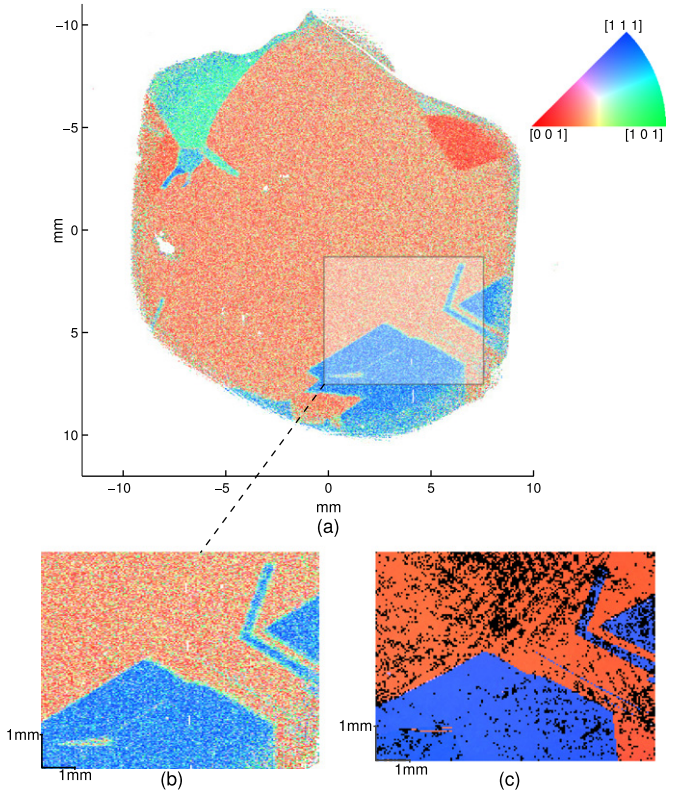

Fig. 2. Inverse pole figures of sample (i) - the full figure obtained using SRAS measurements (a). A section of the sample imaged using both SRAS (b) and EBSD (c) is shown. The same inverse pole figure key is used in all three images.

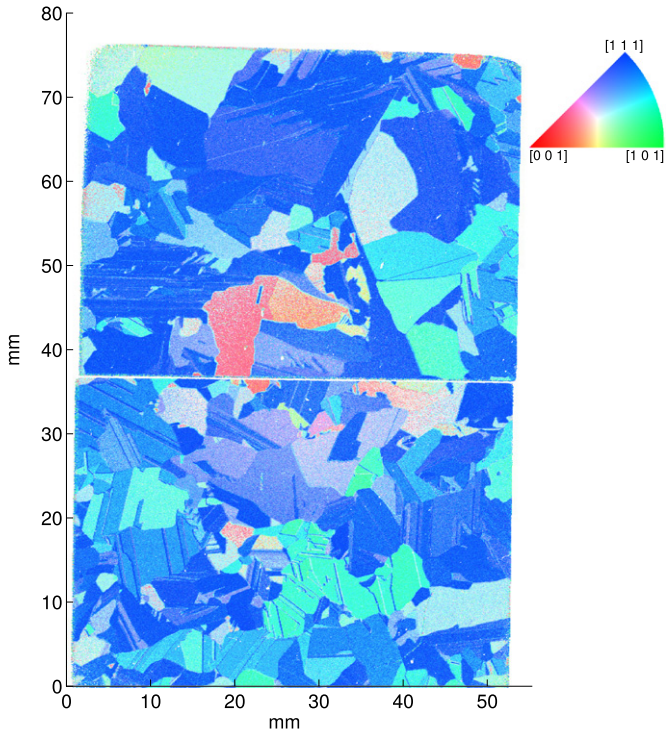

Fig. 3. Inverse pole figure of sample (ii). The image shows the grain orientation on two prepared 52mm × 38mm silicon solar cells. The image shows the microstructure with a preferential grain growth towards the ⟨111⟩ direction.

in Fig. 2 (c). The EBSD scan contains 164 × 123 measurement points and took ∼90 min to complete. The results from both figures show good agreement; the large top grain (orange) and the smaller bottom grain (blue) have Euler angles [112.0°, 14.5°, 86.6°] and [30.7°, 44.4°, 46.4°] in the EBSD scan respectively, which compares with the average Euler angles [121.8°, 20.9°, 69.8°] and [45.9°, 50.1°, 48.7°] obtain using SRAS respectively.

The difference in angles between the two techniques are less than 16°. Part of the reason behind the discrepancy between the two sets of measurements could be due to the number of rotational scans taken. Previous publications have indicated that scanning 18 directions could reduce the difference between data obtained using SRAS and EBSD to ∼6° [20,23].

5. Discussion

In this paper, a demonstration of SRAS's ability to map the microstructure of material by generating and measuring surface acoustic waves is given. The instrument is non-destructive, non-contact, scalable, is able to rapidly collect data, and can be made safe and compact for a manufacturing environment. The system used in this study was not designed specifically for working on silicon - the commercially obtained silicon cells required preparation in order to be characterised.

It is possible to redesign the SRAS system so that measurements could be made on silicon in-situ. For example, switching the generation and detection laser to a pulsed 532 nm and a CW 1064 nm source respectively, would allow direct generation and detection without the need of a chromium layer. To increase the data acquisition and analysis speed, the scanning strategy can be changed from full to representative - once an initial scan identifies the sample's grain boundaries, full rotational velocity information is only required at some sample points within each grain to produce a representative orientation map. The total gain in speed would depend on the size and number of the grains. Additionally, the number of rotations per measurement point could be reduced at a cost of orientation angle accuracy. If there is a possibility of grain rotation within a sample, this will be evident on the representative scan as the measured SAW velocity will gradually change within the grain. A 'smart' scan strategy could be employed: in addition to measuring representative points near the centre of a grain, further measurements could be made around the edges of grains to quantify the degree of rotation of the grain.

Other physical changes to the system could be used to improve acquisition speed including changing the translation equipment, increasing the repetition rate of the pulsed laser and decreasing the computation time required for processing the data.

The results presented in this paper show the potential that SRAS has for inspecting silicon wafers, with notable advantages over other grain measurement techniques that include the ability to perform rapid high resolution full orientation scans whilst accommodating large measurement areas. The instrument, if integrated, could be a valuable in-situ inspection tool for silicon wafer manufacturers, especially as part of developing process control.

Links have been made between certain preference grain growth directions, the section of an ingot that contains these grains and the efficiency of the resultant wafer - the grains normal of wafers varies with section heights when casting, where uppermost sections contain a predominant normal grain direction of ⟨111⟩ [6]. Wafers sliced from this section have been reported to be less efficient - the inexpensive commercial cell scanned and shown in Fig. 3 appears to be such a wafer slice.

Potentially, there could be a greater scope for using this technique to make online measurements of silicon grains during the

solidification process. Data obtained this way could be fed back in the manufacturing process to control the microstructure, eventually leading to silicon cells with higher efficiency yields.

Acknowledgments

This work was supported by the Engineering and Physical Sciences Research Council [grant numbers EP/K021877/1, EP/G061661/1].

References

[1] ITRPV, International Technology Roadmap for Photovoltaic (ITRPV) 2015 Results (accessed Jun 2017). http://www.itrpv.net/Reports/Downloads/.
[2] F. Schindler, J. Schon, B. Michl, S. Riepe, P. Krenckel, J. Benick, F. Feldmann, M. Hermle, S.W. Glunz, W. Warta, M.C. Schubert, IEEE J. Photovoltaics 5 (2015) 1571. http://dx.doi.org/10.1109/JPHOTOV.2015.2466474.
[3] M.A. Green, K. Emery, Y. Hishikawa, W. Warta, E.D. Dunlop, Prog. Photovoltaics, Res. Appl. 24 (2016) 3. http://dx.doi.org/10.1002/pip.2728.
[4] A.K. Ghosh, C. Fishman, T. Feng, J. Appl. Phys. 51 (1980) 446. http://dx.doi.org/10.1063/1.327342.
[5] A.K. Ghosh, A. Rose, H.P. Maruska, D.J. Eustace, T. Feng, Appl. Phys. Lett. 37 (1980) 544. http://dx.doi.org/10.1063/1.91980.
[6] P.C. Hjemås, O. Lohne, A. Wandera, H.S.i.n.g.h. Tathgar, Solid State Phenom. 95 (2004) 217. http://dx.doi.org/10.4028/www.scientific.net/SSP.95-96.217.
[7] T. Kieliba, S. Riepe, W. Warta, J. Appl. Phys 100 (2006) 063706. http://dx.doi.org/10.1063/1.2338126.
[8] H.C. Sio, T. Trupke, D. Macdonald, J. Appl. Phys 116 (2014) 244905. http://dx.doi.org/10.1063/1.4904963.
[9] S. Würzner, R. Helbig, C. Funke, H.J. Möller, J. Appl. Phys 108 (2010) 083516. http://dx.doi.org/10.1063/1.3488643.
[10] B. Ryningen, G. Stokkan, M. Kivambe, T. Ervik, O. Lohne, Acta Mater. 59 (2011) 7703. http://dx.doi.org/10.1016/j.actamat.2011.09.002.
[11] H. Horstmann, C. Körber, K. Sätzler, D. Aydin, T. Kuner, PLoS ONE 7 (2012) e35172. http://dx.doi.org/10.1371/journal.pone.0035172.
[12] M.I. Bertoni, D.P. Fenning, M. Rinio, V. Rose, M. Holt, J. Maser, T. Buonassisi, Energ. Environ. Sci. 4 (2011) 4252. http://dx.doi.org/10.1039/c1ee02083h.
[13] Intego GmbH, GEMINI Grain Analysis (accessed Jun 2017). http://www.intego.de/en/solar/ingots/wafer/gemini-grain-analysis.
[14] D. Lausch, M. Gläser, C. Hagendorf, J. Appl. Phys. 114 (2013) 194509. http://dx.doi.org/10.1063/1.4832782.
[15] C. Funke, T. Behm, R. Helbig, E. Schmid, S. WüRzner, J. Microsc. 246 (2012) 70. http://dx.doi.org/10.1111/j.1365-2818.2011.03588.x.
[16] A. Stoffers, O. Cojocaru-Mirédin, W. Seifert, S. Zaefferer, S. Riepe, D. Raabe, Prog. Photovoltaics Res. Appl. 23 (2015) 1742. http://dx.doi.org/10.1002/pip.2614.
[17] F.J. Humphreys, J. Mat. Sci. 36 (2001) 3833. http://dx.doi.org/10.1023/A:1017973432592.
[18] T. Lehmann, M. Trempa, E. Meissner, M. Zschorsch, C. Reimann, J. Friedrich, Acta Mater. 69 (2014) 1. http://dx.doi.org/10.1016/j.actamat.2014.01.050.
[19] S.D. Sharples, M. Clark, M.G. Somekh, Optics Express 14 (2006) 10435. http://dx.doi.org/10.1364/OE.14.010435.
[20] W. Li, S.D. Sharples, R.J. Smith, M. Clark, M.G. Somekh, J. Acoust. Soc. Am. 132 (2012) 738. http://dx.doi.org/10.1121/1.4731226.
[21] R.J. Smith, W. Li, J. Coulson, M. Clark, M.G. Somekh, S.D. Sharples, Meas. Sci. Technol 25 (2014) 055902. http://dx.doi.org/10.1088/0957-0233/25/5/055902.
[22] R.F.S. Hearmon, Elastic, Piezoelectric, Pyroelectric, Piezooptic, Electrooptic Constants and Nonlinear Dielectric Susceptibilities of Crystals, Landolt-Bornstein New Series Group III, vol. 11. 1979.
[23] W. Li, Laser Ultrasonic Method for Determination of Crystallographic Orientation of Large Grain Metals by Spatially Resolved Acoustic Spectroscopy (SRAS), PhD thesis. University of Nottingham. 2012, http://eprints.nottingham.ac.uk/id/eprint/12391.